Investigation of the Dynamics of a Multibody Wave Energy Converter excited by Regular and Irregular Waves

Marten Hollm[a,*], Leo Dostal[a], Joshua Höhne[a], Daniil Yurchenko[b], Robert Seifried[a]

[a] *Institute of Mechanics and Ocean Engineering, Hamburg University of Technology, 21073 Hamburg, Germany*
[b] *Institute of Sound and Vibration Research, University of Southampton, Highfield, Southampton SO17 1BJ, UK*

Abstract

The dynamics and the performance of a novel multibody wave energy converter is investigated, which is based on inclined single modules connected to a frame. The frame floats on the sea surface and the modules each move translationally along inclined guidance rods. Direct-drive linear generators or rotation based generators convert the relative translational motion between the frame and the modules into electrical power. This paper studies the conditions which influence the performance of the converters in regular and irregular waves. Different design layouts are investigated numerically, whereby the wave excitation is modelled by a random non-white Gaussian stochastic process.

Keywords: wave energy converter, fluid structure interaction, random waves, nonlinear dynamics, energy conversion

1. Introduction

In the view of increasing global energy demand and advancing climate change, it is necessary to explore new sustainable alternatives for energy generation that replace fossil fuels. In the course of the energy transition,

*Corresponding authors
Email address: marten.hollm@tuhh.de (Marten Hollm)

renewable energies from wind, sun and water are becoming increasingly important and are already being used commercially in a variety of ways. In addition to these well-known examples of renewable energy generation, energy can also be obtained from ocean waves. Because of its high power density compared to solar and wind energy, wave energy is also promising for power generation [1]. Therefore, several new wave energy converter (WEC) concepts have been investigated in the last years, cf. [2, 3, 4, 5, 6, 7]. Moreover, many ways to harvest energy from water waves are summarized in [8]. However, since water waves are irregular and most of the wave energy is contained in low-frequency waves, only a small amount of energy has been extracted from ocean waves so far.

A well-known type of wave energy converters (WEC) are the so-called point absorbers, which possess small dimensions compared to the wavelength of the incoming waves. There are different kinds of point absorbers. For example, they can move along the sea surface [6] or be submerged under the water waves, excited by pressure difference [7]. Thereby, point absorbers differ in the number of components from whose motion energy can be extracted.

In the first generation, point absorbers have been developed using a single-body, which oscillates in heave. Examples for these constructions can be found in [6, 9]. However, it has been found that these systems can only harvest an optimal amount of energy if the natural frequency of these systems and the frequency of the incoming waves correspond to each other [10, 11, 12]. As the frequencies of the incoming waves are typically very low ($0.1\,\mathrm{Hz} - 0.2\,\mathrm{Hz}$), the dimensions of the mechanical system have to be impractically large, cf. [13].

In order to enhance the magnitude of harvested wave energy, in [14] it has been studied the behavior of a guided inclined point absorber in regular waves. It has been shown that by varying the inclination angle, the gained power can be enlarged significantly. Moreover, the magnitude of wave energy has been increased by developing two-body WECs, where energy is harvested through the relative motion between the components, cf. [15, 16]. Furthermore, multibody WECs exist, which consist of several moving components. One example for such a multibody WEC has been developed by SINN-Power [17]. It consists of generators mounted on a frame, which each are excited by a moving cylindrical floating body (CFB). Thereby, all CFBs are vertically mounted to the frame.

In this study, the mechanical system of SINN-Power type is generalized by introducing varying inclination angles. The influence of inclination angles

and number of CFBs on power performance of the device is investigated. The CFBs move along the guidances attached on the frame and thereby harvest energy, resulting in additional damping. Since the relative motion between the CFBs and the frame is linear, a direct-drive linear generator can be used for energy harvesting, cf. [18, 19]. But also the use of rotation based generators for energy harvesting is possible. The results presented in this paper for the multibody WEC consider thereby the case of excitation by a regular and non-white Gaussian random process, which can for example be encountered in real sea states.

It has to be noted that the considered multibody WEC can freely float on the sea surface. This is an advantage, since no connection to the environment is needed to harvest energy, in contrast to the system shown in [14]. The multibody WEC presented in this study does not need this connection, since energy is harvested from the relative motion between the frame and the CFBs. Therefore, the location of operation of the WEC is not limited to coastal regions or the neighborhood of offshore systems, but the WEC can operate everywhere at the surface of the ocean. With the WEC presented in this study, the idea of introducing an inclination angle, which greatly increased the amount of harvested energy in [14], can also be used on the open sea surface.

The content of this work is as follows: First, the investigated mechanical system is introduced and the generalized equations of motion are presented. Thereby, the fluid structure interaction and the involved hydrodynamic forces are considered for the case of regular waves. Then, the modeling of irregular waves and the corresponding modeling of response of the mechanical structure are presented. Afterwards, the harvested energy is computed for different inclination angles and numbers of CFBs in order to analyze the corresponding energy harvesting performance. Thereby, regular as well as irregular seas are considered. Finally, this work ends with a conclusion.

2. Mechanical System

In this section, the mechanical system is introduced and the general equation of motion is presented. Thereby, the applied forces are described and the hydrodynamic forces are calculated for the case of an excitation by regular waves.

2.1. Description of the mechanical system

The mechanical system consists of a frame and N CFBs. Figure 1 shows the side view of the structure for the case of $N = 4$ in still water and in the presence of water waves. In this work, the motion of the system in the xy-plane is considered, whereby x denotes the horizontal and y the vertical coordinates, respectively. Each CFB moves between the upper and lower beam of the frame along guidance rods with corresponding displacement ξ_i in a plane, which is inclined to the frame by the corresponding adjustable inclination angle ε_i, $i \in \{1, \ldots, N\}$. The frame can freely move in the xy-plane, whereby the angle of rotation is denoted by β. The horizontal and vertical displacements of the geometric center C of the frame are denoted by x_F and y_F, respectively. Thereby, all displacements refer to the equilibrium position in still water, at which x_F, y_F, β and ξ_i are zero.

In the direction of ξ_i, the CFBs and the frame are connected by springs. Mechanical friction acting between the frame and the CFBs is accounted for by a velocity dependent damping force. In order to simplify the problem, it is assumed that the motion of the CFBs is not limited by the geometry of the frame, i.e. the CFBs can move without colliding with the frame.

Direct-drive linear generators or rotation based generators can then convert the relative motion between the CFBs and the frame to electrical energy.

2.2. General equations of motion

Let

$$\mathbf{z} = [x_\mathrm{F}, y_\mathrm{F}, \beta, \xi_1, \ldots, \xi_N]^\mathrm{T} \tag{1}$$

be the vector consisting of all generalized coordinates of the multibody WEC. The general equations of motion of the mechanical system can then be written as

$$\mathbf{M}(\mathbf{z}, t)\ddot{\mathbf{z}} + \mathbf{k}(\mathbf{z}, \dot{\mathbf{z}}, t) = \mathbf{q}(\mathbf{z}, \dot{\mathbf{z}}, t), \tag{2}$$

whereby t is the time, $\mathbf{M}$ is the generalized mass matrix, $\mathbf{k}$ is the vector of Coriolis, centrifugal and gyroscopic forces and $\mathbf{q}$ is the vector of the applied forces. Thereby, $\mathbf{q}$ includes the stiffness and mechanical damping force $F_{\mathrm{sd},i}$, which acts on the CFB $i \in \{1, \ldots, N\}$ in the direction of ξ_i. In this study, it is computed by

$$F_{\mathrm{sd},i} = k_\mathrm{s}(l_{0,i} - l_i + \xi_i) + d_\mathrm{m}\,\dot{\xi}. \tag{3}$$

Here, k_s is the linear stiffness coefficient and d_m is the linear damping coefficients due to mechanical friction. The term $k_\mathrm{s}(l_{0,i} - l_i)$ represents the preload

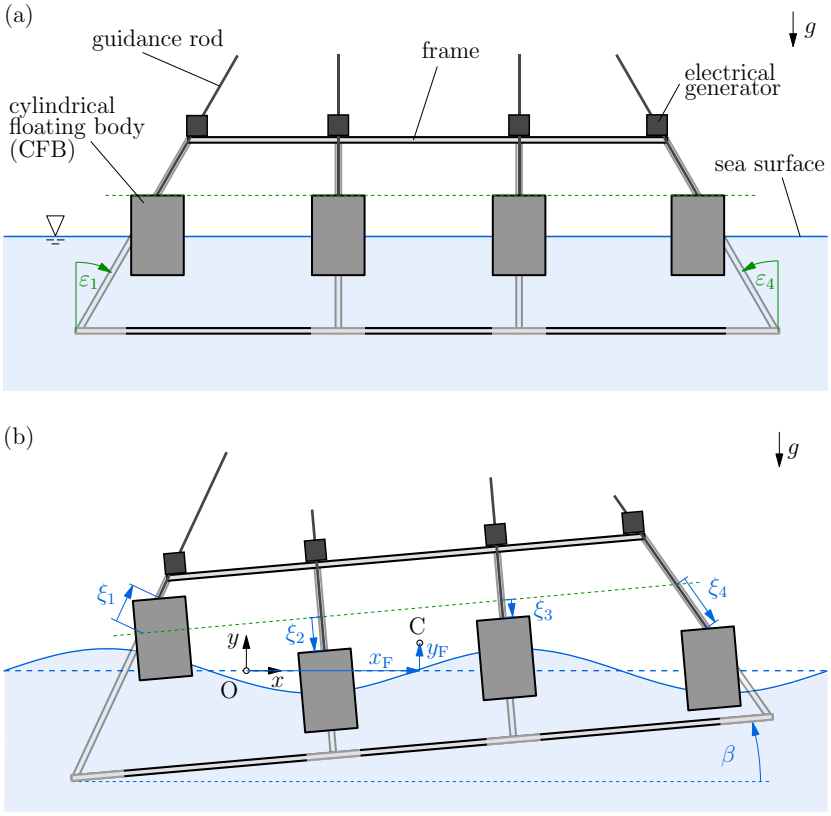

Figure 1: Sketch of the mechanical system in still water position (a) and in the presence of harmonic water waves (b).

force of the spring, whereby $l_{0,i}$ is the unloaded and l_i the preloaded length of the spring, respectively.

2.3. Hydrodynamic forces in regular waves

In order to compute the hydrodynamic forces acting on each CFB, the water pressure p has to be integrated over the corresponding wetted surfaces. Assuming an irrotational, unsteady flow, the water pressure p can be computed using potential flow theory and Bernoulli's equation,

$$p(x, y, z, t) = -\rho \frac{\partial \Phi(x, y, z, t)}{\partial t} - \rho_{\mathrm{w}} g y, \tag{4}$$

where Φ is the velocity potential, ρ_{w} is the density of water and g is the gravity constant. In Eq. (4), a linearisation in Φ has been carried out.

For incoming harmonic water waves with wave frequency ω and wave amplitude A, the corresponding sea surface displacement is given by

$$\eta(x,t) = \mathrm{Re}\{A\exp(\mathrm{i}(\kappa x - \omega t))\} \quad \text{with} \quad \omega^2 = \kappa g \tanh(\kappa h), \tag{5}$$

whereby κ denotes the wave number and h the water depth.

Following [20] the corresponding velocity potential Φ acting on the $i-$th CFB can be computed by

$$\begin{aligned}\Phi_i(x,y,z,t) =& \mathrm{Re}\{A[\phi_{i,0}(x,y,z) + \phi_{i,7}(x,y,z)]\mathrm{e}^{-\mathrm{i}\omega t} \\ &+ (-\mathrm{i}\omega)\left(\sum_{j=1}^{6}\hat{\zeta}_j\phi_{i,j}(x,y,z)\right)\mathrm{e}^{-\mathrm{i}\omega t}\}.\end{aligned} \tag{6}$$

Here, $\phi_{i,0}$ denotes the incident potential of the incoming waves acting on the $i-$th CFB. The reflections of the incident waves with respect to a non-moving CFB are represented by the corresponding scattering potential $\phi_{i,7}$. Furthermore, $\phi_{i,j}$ denotes the radiation potentials and $\hat{\zeta}_{i,j}$ the respective complex amplitudes of the motion of the $i-$th CFB in the j-th direction. Thereby, $j = 1,2,3$ represent the translational motion of the CFB in the x-,y- and z-direction and $j = 4,5,6$ the rotational motion about the x-,y- and z-axis.

It should be noted that in real applications, the motion of each CFB results in hydrodynamic forces that can affect other CFBs. However, as the distance between CFBs increases, the hydrodynamic interaction forces between the different CFBs become small compared to the forces resulting from the incident waves, radiation potential, and scattering potential. In order to simplify the study, it is assumed that the distance between CFBs is large enough, such that the hydrodynamic interaction forces between different CFBs can be neglected.

The hydrodynamic forces $\mathbf{F}_{\mathrm{Hyd},i}$ and torques $\mathbf{M}_{\mathrm{Hyd},i}$ acting on the $i-$th CFB are given by

$$\mathbf{F}_{\mathrm{Hyd},i} = \iint\limits_{S_{\mathrm{B},i}} p\mathbf{n}\,\mathrm{d}S, \quad \mathbf{M}_{\mathrm{Hyd},i} = \iint\limits_{S_{\mathrm{B},i}} p(\mathbf{r}\times\mathbf{n})\,\mathrm{d}S. \tag{7}$$

Thereby, $S_{\mathrm{B},i}$ denotes the wetted surface of the $i-$th CFB and $\mathbf{n}$ is the normal vector taken to be positive when pointing into the body. Moreover, $\mathbf{r}$ denotes the position vector between the reference point of the torque and

the points on the wetted surface of the CFB. In the following, the index i is dropped to simplify the notation. Inserting Eq. (6) into (7), the hydrodynamic forces $\mathbf{F}^j_{\mathrm{Hyd}}$ and torques $\mathbf{M}^j_{\mathrm{Hyd}}$in the direction j acting on the $i-$th CFB result into

$$\mathbf{F}^j_{\mathrm{Hyd}} = -\sum_{k=1}^{6}\left(\mu_{j,k}\ddot{\zeta}_k + \lambda_{j,k}\dot{\zeta}_k\right) + F^j_{\mathrm{B}} + \mathrm{Re}\left\{AX_j \mathrm{e}^{\mathrm{i}(\kappa x_c - \omega t)}\right\}, \quad j \in \{1,2,3\}, \tag{8}$$

$$\mathbf{M}^j_{\mathrm{Hyd}} = -\sum_{k=1}^{6}\left(\mu_{j,k}\ddot{\zeta}_k + \lambda_{j,k}\dot{\zeta}_k\right) + M^j_{\mathrm{B}} + \mathrm{Re}\left\{AX_j \mathrm{e}^{\mathrm{i}(\kappa x_c - \omega t)}\right\}, \quad j \in \{4,5,6\}. \tag{9}$$

Thereby, ζ_k represents the motion of the CFB in direction k with amplitude $\hat{\zeta}_k$ and x_c is the x-coordinate of the center point of the CFB with respect to the inertial coordinate system. Moreover, $\mu_{j,k}$ and $\lambda_{j,k}$ are the added mass and hydrodynamic damping coefficient acting in direction j due to the motion in direction k, respectively. The buoyancy force as well as the corresponding torque in direction j are represented by F^j_{B} and M^j_{B}, respectively. Finally, the excitation force in direction j is represented by X_j. More details about the corresponding terms can be found in [20].

This work considers a planar motion of the mechanical system, therefore, the forces, torques and motions in j-th direction are zero for $j = 3, 4, 5$. In order to compute the added mass and hydrodynamic damping coefficients as well as the excitation forces in regular waves, the matched eigenfunction method is used. The way of computing these values is presented by Yeung [21] and Garrett [22] for the case of a single truncated cylinder, respectively. Thereby, it is noted that the values of $\mu_{j,k}$, $\lambda_{j,k}$ and X_j depend on the geometry of the corresponding CFB, the immersion depth of the CFB, the water depth h and the wave frequency ω.

3. Mechanical behavior in irregular sea

Since real ocean sea is irregular, any WEC has to be constructed in such a way that a large amount of energy is harvested in random sea. This section describes the modeling of the irregular sea and the modeling of the corresponding system response.

3.1. Modeling of irregular sea

Realistic ocean sea is simulated here by using the superposition principle of harmonic waves. Thereby, water waves with wave frequencies ω and corresponding wave numbers $\kappa(\omega)$ are superposed. With this, the wave amplitudes of each harmonic wave component depends on the underlying sea state. This is given by the corresponding one-sided spectral density $S(\omega)$, cf. [23, 24]. Common sea states are described by the Pierson-Moskowitz spectrum for deep water and the Joint North Sea Wave Project (JONSWAP) spectrum for shallow water waves. Then, a one dimensional irregular long-crested wave surface $Z(x,t)$ can be determined by

$$Z(x,t) = \sum_{n=1}^{N_{\mathrm{comp}}} \cos(\omega_n t - \kappa(\omega_n)x + \psi(\omega_n))\sqrt{2S(\omega_n)\Delta\omega_n}. \tag{10}$$

Here, the sea spectrum is divided in N_{comp} components with respective frequencies $\omega_n \in [\omega_{\mathrm{min}}, \omega_{\mathrm{max}}]$ and widths $\Delta\omega_n$, which do not need to be of same size. Moreover, $\psi(\omega_n)$ is a randomly distributed phase shift in the interval $[0,\, 2\pi]$. Such a modeling results in a linear random sea with Gaussian distributed wave elevation and Rayleigh distributed wave amplitude.

In the following, the obtained results are presented for the Pierson-Moskowitz spectrum, which can be described by the peak frequency ω_{P} and significant wave height H_{s}.

3.2. System response in irregular sea

The behavior of the mechanical system can be computed by solving Eq. (2). For a harmonic wave of frequency ω and amplitude A, the applied hydrodynamic forces and torques can be computed using the Eqs. (8) and (9), respectively. However, irregular sea are described by a sum of harmonic waves, cf. Eq. (10). The question arises how to compute the corresponding hydrodynamic forces acting on the mechanical system.

The hydrodynamic forces due to irregular sea are computed using the approach described in [14]. Therefore, average values for all $\mu_{j,k}$ and $\lambda_{j,k}$ are used by determining the corresponding values at the peak frequency $\omega = \omega_{\mathrm{P}}$. In this way, the response for waves with peak frequency ω_{P} is accurate. Using

$$\bar{\mu}_{j,k} := \mu_{j,k}(\omega_{\mathrm{P}}), \quad \bar{\lambda}_{j,k} := \lambda_{j,k}(\omega_{\mathrm{P}}) \quad \text{for } j,k \in \{1,...,6\}, \tag{11}$$

the hydrodynamic forces $\mathbf{F}^j_{\mathrm{Hyd}}$ and torques $\mathbf{M}^j_{\mathrm{Hyd}}$ in direction j acting on a CFB, which is excited by an irregular sea determined by Eq. (10), are given by

$$\mathbf{F}^j_{\mathrm{Hyd}} = -\sum_{k=1}^{6}\left(\bar{\mu}_{j,k}\ddot{\zeta}_k + \bar{\lambda}_{j,k}\dot{\zeta}_k\right) + F^j_{\mathrm{B}} + \sum_{n=1}^{N_{\mathrm{comp}}} \mathrm{Re}\left\{\sqrt{2S(\omega_n)\Delta\omega_n}X_j(\omega_n)\mathrm{e}^{\mathrm{i}(\kappa(\omega_n)x_c-\omega t+\psi(\omega_n))}\right\}, \quad j\in\{1,2,3\}, \tag{12}$$

$$\mathbf{M}^j_{\mathrm{Hyd}} = -\sum_{k=1}^{6}\left(\bar{\mu}_{j,k}\ddot{\zeta}_k + \bar{\lambda}_{j,k}\dot{\zeta}_k\right) + M^j_{\mathrm{B}} + \sum_{n=1}^{N_{\mathrm{comp}}} \mathrm{Re}\left\{\sqrt{2S(\omega_n)\Delta\omega_n}X_j(\omega_n)\mathrm{e}^{\mathrm{i}(\kappa(\omega_n)x_c-\omega t+\psi(\omega_n))}\right\}, \quad j\in\{4,5,6\}. \tag{13}$$

Thereby, the values of $\bar{\mu}_{j,k}$, $\bar{\lambda}_{j,k}$ and $X_j(\omega_n)$ are determined for the equilibrium position of each cylinder. Here, it is assumed that the CFBs do not perform large amplitude motions in the vertical direction.

3.3. Modeling of power take off system

If energy is harvested from the motion of the CFBs, an additional electrical damping Force F_{el} will be introduced, which acts on the mechanical system. In this work it is assumed that the electrical damping force acting on the i-th CFB depends linearly on the velocity of the CFB, i.e.

$$F_{\mathrm{el},i} = d_{\mathrm{el},i}\dot{\xi}_i, \quad i\in\{1,\ldots,N\}. \tag{14}$$

Thereby, $d_{\mathrm{el},i}$ is the corresponding electrical damping constant.

The damping force leads to the mechanical power $P_{\mathrm{mech},i} = F_{\mathrm{el},i}\dot{\xi}$. This power is related to the electrical power $P_{\mathrm{el},i}$ by means of the efficiency factor $\eta_{\mathrm{eff},i}$, i.e. $P_{\mathrm{el},i} = \eta_{\mathrm{eff},i}\,P_{\mathrm{mech}}$. Therefore, the electrical power harvested from the motion of the i-th CFB can be computed by

$$P_{\mathrm{el},i} = \eta_{\mathrm{eff},i}d_{\mathrm{el},i}\dot{\xi}_i^2, \quad i\in\{1,\ldots,N\}. \tag{15}$$

Using this, the electrical energy harvested from the $i-$th CFB and from the whole system during a time interval $[t_{\mathrm{start}}, t_{\mathrm{end}}]$ is given by

$$E_{\mathrm{el},i} = \int_{t_{\mathrm{start}}}^{t_{\mathrm{end}}} \eta_{\mathrm{eff},i}d_{\mathrm{el},i}\dot{\xi}_i^2\mathrm{d}t, \quad E_{\mathrm{el,total}} = \sum_{i=1}^{N} E_{\mathrm{el},i}, \tag{16}$$

respectively. The corresponding time averaged power $\bar{P}_{\mathrm{el},i}$ of the $i-$th CFB, the time averaged total power $\bar{P}_{\mathrm{el,total}}$ of the system as well as the time averaged total power normalized by the number of CFBs $\bar{P}_{\mathrm{el,mean}}$ is given by

$$\bar{P}_{\mathrm{el},i} = \frac{E_{\mathrm{el},i}}{t_{\mathrm{end}} - t_{\mathrm{start}}}, \quad \bar{P}_{\mathrm{el,total}} = \frac{E_{\mathrm{el,total}}}{t_{\mathrm{end}} - t_{\mathrm{start}}}, \quad \bar{P}_{\mathrm{el,mean}} = \frac{\bar{P}_{\mathrm{el,total}}}{N}, \tag{17}$$

respectively.

4. Numerical results

In this section, the dynamics of the system in regular and irregular sea states are analyzed. Furthermore, the harvested energy of the system is studied for different inclination angles and numbers of CFBs. In order to simplify the study, other system parameters like the masses of the CFBs, the height of the frame, the stiffness and damping coefficients are kept constant.

In the following, results are presented for a frame with a length of 100 m, mass per length of 60 kg/m and a height of 7 m. All CFBs are assumed to have the same geometry and mass. Furthermore, they are equally distributed along the length of the frame and have a diameter of 2 m, a height of 7.5 m and a mean density of 72 kg/m^3. The center of gravity of each CFB is located 1.25 m below the corresponding geometric center point. The remaining used parameters, which have already been introduced in this work, are summarized in Tab. 1. Thereby, the stiffness, damping and efficiency coefficients are the same for all CFBs. In all simulations, the effect of viscous drag forces of the water are neglected. Since these forces are neglected for all considered simulations, the results are still comparable.

In order to further simplify the study of the effects of different inclination angles on the overall performance of the system, only the CFBs at the ends of the frame are inclined. They are inclined by the same angle ε to the outside of the frame. In this way, the system becomes also symmetric. Thereby, an angle is positive if the rotation is anticlockwise. An example for a system with $N = 4$ CFBs is shown in Fig. 1a with $\varepsilon_1 = -\varepsilon$, $\varepsilon_4 = \varepsilon$, $\varepsilon_2 = \varepsilon_3 = 0$.

In all numerical simulations, Eq. (2) is solved with zero displacements and velocities initial conditions, i.e. $\mathbf{z}(t = 0) = \mathbf{0}$, $\dot{\mathbf{z}}(t = 0) = \mathbf{0}$.

4.1. Results for regular waves

In order to get a first impression of the system behavior in regular waves, Fig. 2 shows the response for regular waves with amplitude $A = 0.5\,\mathrm{m}$

Table 1: Parameters used in all simulations.

g [m/s^2]	ρ_w [kg/m^3]	h [m]	k_s [N/m]	d_m [Ns/m]	d_el [Ns/m]	η_eff [−]
9.81	1023	20	2000	2000	1000	0.8

and wave frequency $\omega = 1\,\mathrm{rad/s}$ for the time period of 5000 s. Thereby, an inclination angle of $\varepsilon = 30°$ and $N = 5$ CFBs are used with $\varepsilon_1 = -\varepsilon$, $\varepsilon_5 = \varepsilon$, $\varepsilon_2 = \varepsilon_3 = \varepsilon_4 = 0$.

Figures 2a-e present the temporal behavior of the frame. As it is shown in Fig. 2a, the frame moves in the positive x-direction. Moreover, Figs. 2b and c show the temporal behavior of the response in the y-direction and the rotation angle β in blue. In order to better visualize the temporal behavior of the respective amplitudes, the corresponding envelopes of the responses are shown in orange. It can be seen that the amplitude of both responses increases in the first 2000 s. After this time, the corresponding response amplitudes converge to constant values. In order to get a better insight into the temporal behavior of y_F and β, the values of y_F and β are shown in Fig. 2d and e for the time interval $[3970\,\mathrm{s}, 4030\,\mathrm{s}]$, respectively. Again, it can be seen that the amplitude of y_F and β becomes constant after 2000 s. This shows that the overall dynamic behavior of the frame for the used sea and system parameters is represented in a time interval with a duration of 5000 s.

The corresponding displacements of all CFBs are presented in Fig. 2f for the time interval $[3970\,\mathrm{s}, 4030\,\mathrm{s}]$. It can be seen that in this time interval, where the amplitudes of y_F and β are constant, each of the CFBs also moves with a constant amplitude. However, different CFBs show different amplitudes in their motions, which results from the corresponding motion of the frame with respect to the water wave. At this point it is recalled that only the CFBs with the corresponding displacements ξ_1 and ξ_5 are inclined by the angle $\varepsilon_1 = -\varepsilon$ and $\varepsilon_5 = \varepsilon$ with $\varepsilon = 30°$, respectively. The other CFBs with the respective displacements ξ_2, ξ_3 and ξ_4 are oriented vertically with respect to the frame, i.e. by $\varepsilon_2 = \varepsilon_3 = \varepsilon_4 = 0°$. Moreover, Fig. 2f shows that all CFBs have the same frequency, which is the same as for y_F and β. However, this frequency is different from the wave frequency, which results from the forward motion of the frame.

Since the motions of the CFBs have the same frequency but differ in their amplitude, the corresponding velocities differ also in their amplitude. This can be seen in Fig. 2g, where the velocities of all CFBs are depicted for

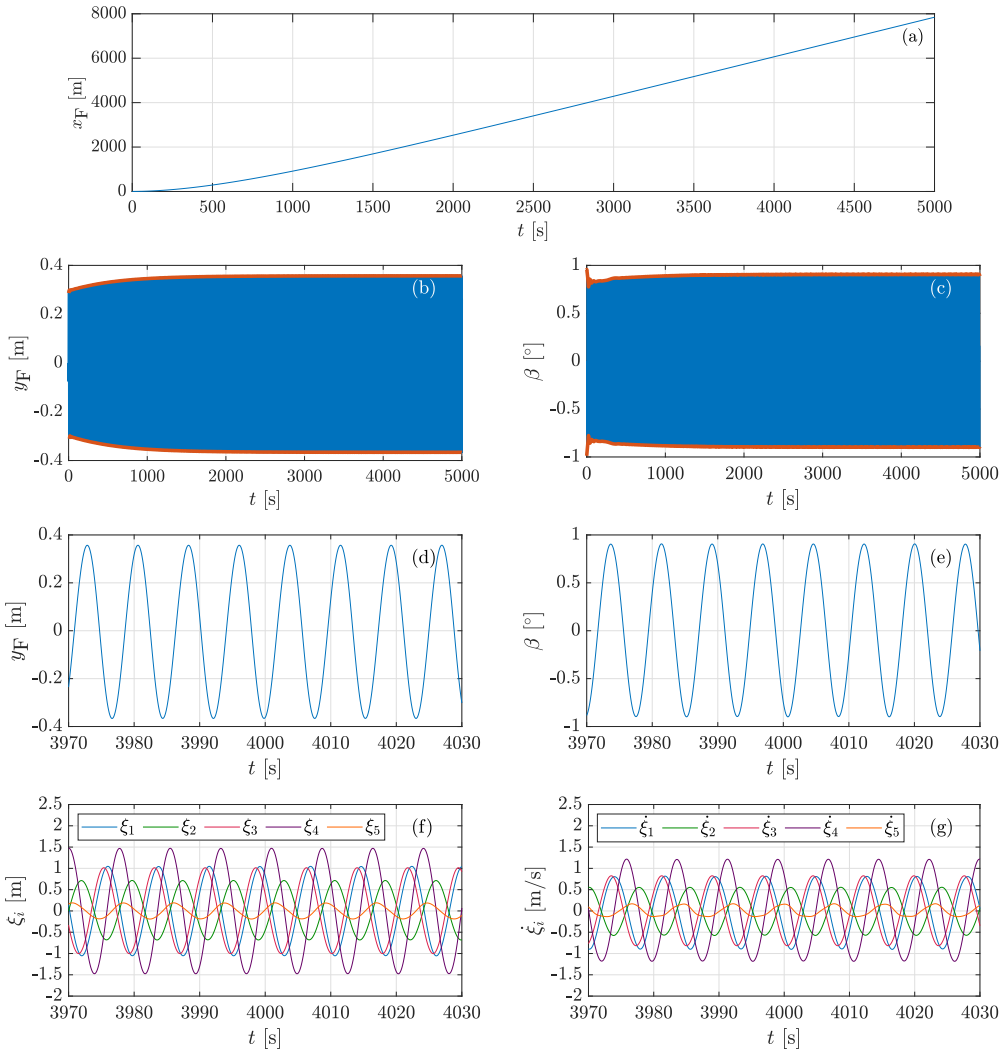

Figure 2: Temporal behavior of the mechanical system. The system is excited by a regular wave with amplitude $A = 0.5\,\mathrm{m}$ and frequency $\omega = 1\,\mathrm{rad/s}$. The motion of the frame is represented by the corresponding displacement x_F in x-direction (a), y_F in y-direction (b) and rotation angle β (c). In (d) and (e), the corresponding values of y_F and β are shown for the time interval $[3970\,\mathrm{s}, 4030\,\mathrm{s}]$. The displacement and velocities of all CFB are depicted in (f) and (g), respectively.

the time interval $[3970\,\mathrm{s}, 4030\,\mathrm{s}]$. Resulting from this and Eq. (15), the CFBs harvest different amounts of energy. This is presented in Fig. 3a, which shows the corresponding harvested energy $P_{\mathrm{el},i}(t)$ of each CFB with respect to time.

The resulting time averaged power $\bar{P}_{\mathrm{el},i}$ of each CFB is shown in Fig. 3b. Since all CFBs move with the same frequency, a higher amplitude of motion of the CFB results in a higher amount of harvested energy. The harvested time averaged total energy of the whole system is $\bar{P}_{\mathrm{el,total}} = 1275\,\mathrm{W}$, whereby in average each cylinder harvests $\bar{P}_{\mathrm{el,mean}} = 255\,\mathrm{W}$. For time averaging, the time interval $[t_{\mathrm{start}}, t_{\mathrm{end}}] = [2000\,\mathrm{s}, 5000\,\mathrm{s}]$ is taken into account. Here, the system moves in a steady state.

Next, the influence of the inclination angle and the number of CFBs on the harvested energy is investigated. Thereby, the system moves in regular waves. Figure 4 presents the power $\bar{P}_{\mathrm{el,mean}}$ at the frequency ω of the incoming waves and the inclination angle ε. Thereby, different numbers of CFBs are taken into account. Here, only odd values for N are taken into account, since then one of the CFBs is located near the center of the frame. Therefore, this CFB introduces only a small inertia into the system. As a result, the system performs larger rotations β. In order to give an overview of the different setups of the investigated systems, the angles of inclination of the CFBs and the distances between the evenly spaced CFBs are summarized in Tab. 2.

It can be seen that for all considered numbers of CFBs, a high amount of energy can be harvested for frequencies around 3 rad/s. However, waves with frequencies lower than 2 rad/s generally occur in real oceans. For these low frequencies, it is shown that more energy can be harvested from the system if a higher number of CFBs is used. Therefore, more CFBs can increase the chance of harvesting a higher amount of energy. However, a higher number of CFBs also leads to an increasing inertia of the system and costs for construction. Therefore, the number of CFBs must be chosen wisely.

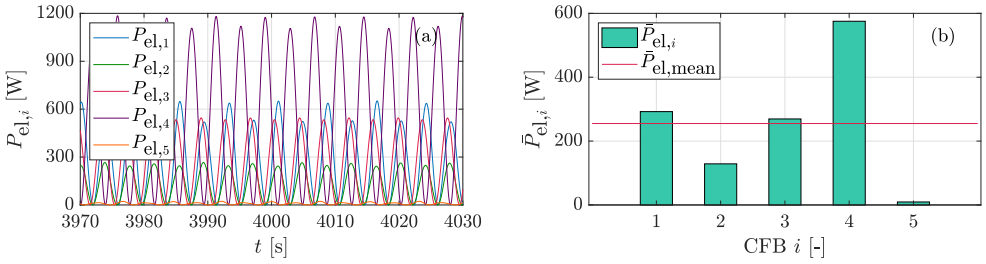

Figure 3: Harvested power of the mechanical system. The system is excited by a regular wave with amplitude $A = 0.5\,\mathrm{m}$ and frequency $\omega = 1\,\mathrm{rad/s}$. For the time interval $[3970\,\mathrm{s}, 4030\,\mathrm{s}]$, the harvested power of each of the CFBs is depicted in (a). The resulting time averaged total power related to each CFB is shown in (b).

Table 2: Inclination angles and distances between the evenly spaced CFBs.

Number of CFBs	ε_1 [−]	ε_2 [−]	ε_3 [−]	ε_4 [−]	ε_5 [−]	ε_6 [−]	ε_7 [−]	equal space between CFBs [m]
3	$-\varepsilon$	0	ε	−	−	−	−	33.33
5	$-\varepsilon$	0	0	0	ε	−	−	20.00
7	$-\varepsilon$	0	0	0	0	0	ε	14.29

Studying the effect of the inclination angle, it can be seen that an angle of 0° leads in general to the highest amounts of energy. However, increasing the inclination angle leads to local maxima in the harvested energy. One of these local maxima is found for the parameter combination $N = 5$, $\varepsilon = 20°$, $\omega = 3\,\mathrm{rad/s}$, cf. Fig. 4b. In this case more energy can be harvested as for $N = 5$, $\varepsilon = 0°$, $\omega = 3\,\mathrm{rad/s}$. This indicates that the introduction of an inclination angle can increase the amount of harvested energy in special cases.

It has to be noted that a study on the influence of inclination angles has been performed in [14] for the case of just one CFB. There, the authors conclude that the highest amount of power can be harvested at an inclination angle of about $\varepsilon = 45°$. This seems to contradict the results of this study, in which the largest amount of power is harvested at small inclination angles. However, the system studied in [14] is fixed, i.e. the CFB is moving with respect to a fixed guidance. The position of the frame in the horizontal direction and the corresponding position of the water wave crest affect the displacements of the CFBs, see Fig. 2f. This also influences the amount of harvested power.

Moreover, it has to be noted that these simulation results are all related to the considered mechanical system. No optimization process has been performed to increase the amount of harvested energy. However, a large amount of energy is actually only harvested for frequencies higher than $2\,\mathrm{rad/s}$, which occur in the open sea only with a small amplitude and energy. In order to increase the harvested energy for waves occurring in real seas, an optimization process should be performed. As has been indicated, inclined CFBs can increase the amount of harvested energy and should therefore be taken into account in the optimization process.

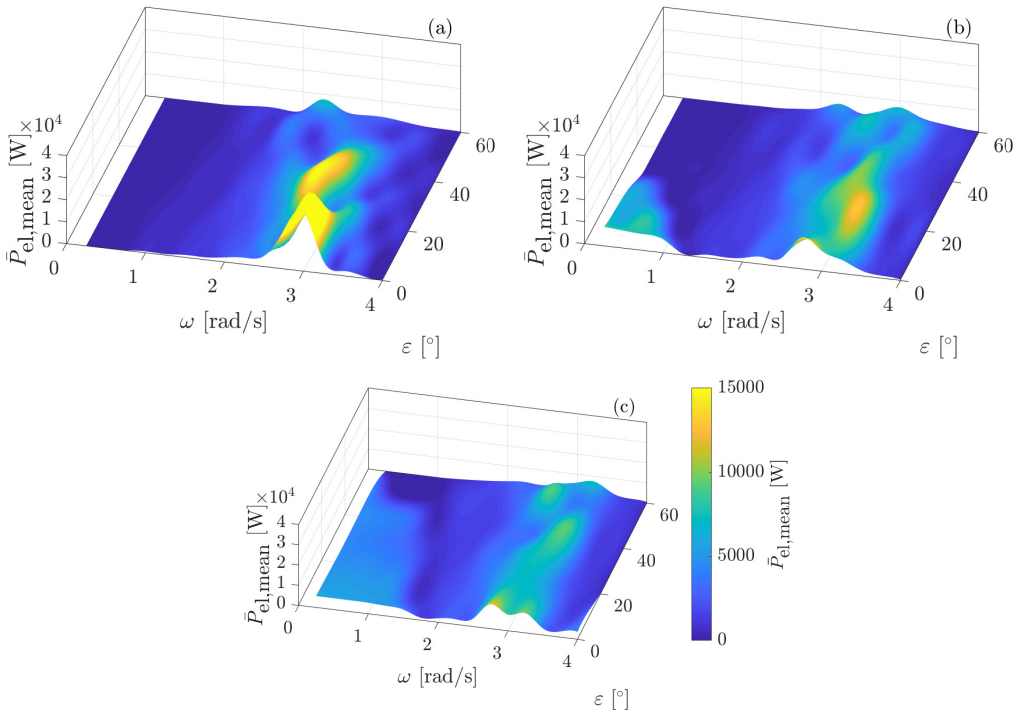

Figure 4: Harvested time averaged total power normalized by the number of CFBs, $\bar{P}_{\mathrm{el,mean}}$. The power is presented against the wave frequency ω of the harmonic waves and the inclination angle ε of the CFBs positioned at the ends of the frame. The results are shown for (a) $N = 3$, (b) $N = 5$ and (c) $N = 7$ CFBs, respectively. All incoming regular waves have an amplitude of $A = 0.5\,\mathrm{m}$.

4.2. Results for irregular waves

In the following, the amount of harvested energy from the mechanical system moving in random seas is studied. Irregular ocean waves are generated using Eq, (10), whereby the amplitude of the waves are computed using the Pierson-Moskowitz spectrum with a corresponding significant wave height of $H_{\mathrm{s}} = 2\,\mathrm{rad/s}$ and peak frequencies $\omega_{\mathrm{P}} \in [0.25\,\mathrm{rad/s}, 4\,\mathrm{rad/s}]$. Irregular seas are generated by superposing $N_{\mathrm{comp}} = 100$ harmonic wave components with respective wave frequencies ω_n and phase shifts $\psi(\omega_n) \in [0, 2\pi]$, $n \in \{1, \ldots, N_{\mathrm{comp}}\}$.

The temporal behavior of the mechanical system is simulated for different numbers of CFBs and peak frequencies ω_{P} over a duration of 100000 s. For time averaging of the corresponding harvested energy, the time interval

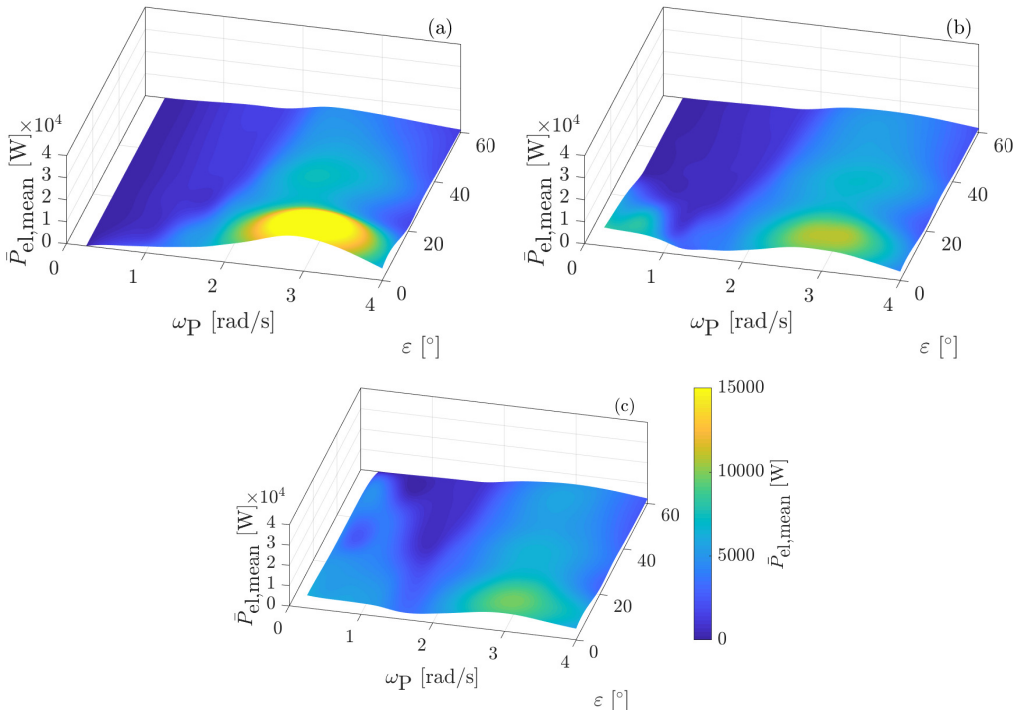

Figure 5: Harvested time averaged total power normalized by the number of CFBs, $\bar{P}_{\mathrm{el,mean}}$. The power is presented against the peak frequency ω_{P} of the irregular waves and the inclination angle ε of the CFBs positioned at the ends of the frame. The results are shown for (a) $N = 3$, (b) $N = 5$ and (c) $N = 7$ CFBs, respectively. In order to generate the irregular seas, a significant wave height of $H_{\mathrm{s}} = 2\,\mathrm{m}$ is used and $N_{\mathrm{comp}} = 100$ harmonic waves are superposed.

$[t_{\mathrm{start}}, t_{\mathrm{end}}] = [2000\,\mathrm{s}, 100000\,\mathrm{s}]$ is used.

The corresponding results for the harvested time averaged total power normalized by the number of CFBs, $\bar{P}_{\mathrm{el,mean}}$, are presented in Fig. 5. Thereby, $N = 3$, $N = 5$ and $N = 7$ CFBs are used, respectively. Information about the setups of the three different mechanical systems can be found in Tab. 2. For all considered numbers of CFBs it is shown that a large amount of energy can be harvested for sea states consisting of harmonic waves with high frequencies, i.e. for large values of ω_{P}, e.g. $\omega_{\mathrm{P}} = 3, \mathrm{rad/s}$. For smaller values of ω_{P}, energy can only be harvested for a high number of CFBs, cf. Fig. 5c.

Regarding the inclination angle ε, it is shown that in general a smaller value of ε leads to a larger amount of energy. However, as can also be seen for

the case of regular wave excitation, a variation of the inclination angle leads to local maxima in the harvested energy. Thereby, in the irregular waves, one maximum is dominating, see for example Fig. 5a.

Again, it has to be noted that these simulation results are all related to the considered mechanical system. No optimization process has been performed to increase the amount of harvested energy, especially not for smaller peak frequencies ω_P. It has already been indicated that the inclined CFBs can increase the amount of harvested energy and should therefore be taken into account in an optimization process.

Comparing Fig. 4 and Fig. 5, it is noticed that smaller maximal amounts of power can be harvested from irregular seas than from regular seas. This can also be seen in Tab. 3, which summarizes the maximal amounts of powers harvested from the mechanical systems with $N = 3$, $N = 5$, and $N = 7$ CFBs, respectively. However, for most combinations of inclination angles and excitation frequencies, the mechanical system is able to harvest more energy from irregular seas than from regular seas. This can be seen in Fig. 6, where the harvested energies are compared for all considered cases. The much bigger blue regions in Figs. 6b, d and f indicate that for most combinations of inclination angles and excitation frequencies, larger amounts of energy are harvested from irregular seas than from regular waves. Moreover, Fig. 6 shows that the corresponding value of $\bar{P}_\mathrm{el,mean}$ harvested from irregular sea is not as sensitive against changing sea and system conditions as for regular waves. This means that for changing parameters, the value of $\bar{P}_\mathrm{el,mean}$ does not have as big fluctuations in irregular seas as in regular seas.

Regarding the results in the current study, the setup with 7 CFBs shows the best results, since energy can be harvested for smaller values of ω_P. That energy can be harvested for smaller values of ω_P is fundamental for a wave energy converter. In the real ocean only sea states with smaller values of ω_P occur with high amplitudes, from which high amounts of energy can be

Table 3: Maximal values of harvested power $\bar{P}_\mathrm{el,mean}$ from regular and irregular seas for different numbers of CFBs.

Number of CFBs	$\max\{\bar{P}_\mathrm{el,mean}\}$ in regular waves [W]	$\max\{\bar{P}_\mathrm{el,mean}\}$ in irregular waves [W]
3	30663	18569
5	14591	9940
7	12178	9811

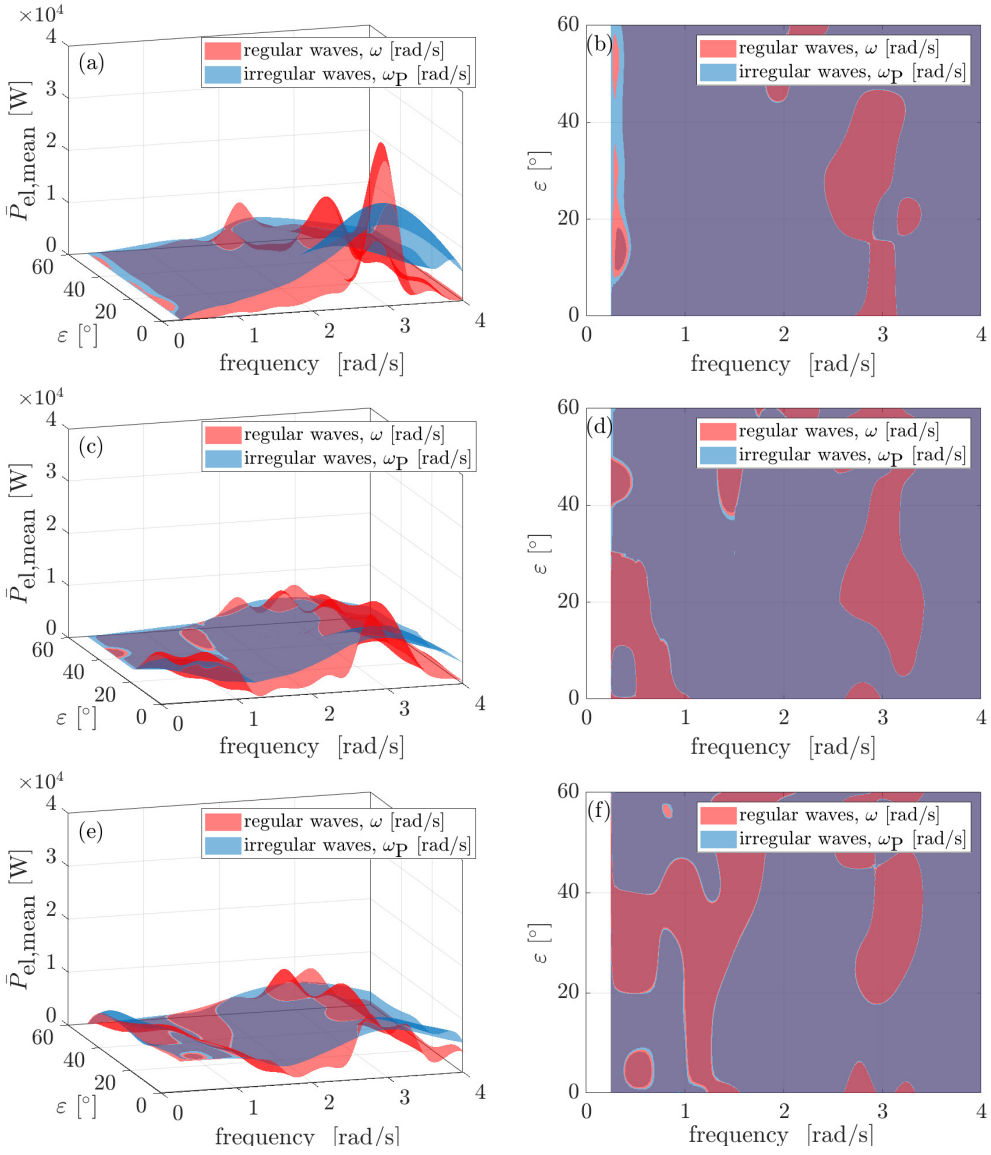

Figure 6: Comparison of the results shown in Figs. 4 and 5. The power is presented against the wave frequency ω for regular and peak frequency ω_{P} for irregular waves. The respected results are shown for (a-b) $N = 3$, (c-d) $N = 5$ and (e-f) $N = 7$ CFBs from two different points of view.

harvested

In order to increase the harvested power in the presence of waves with low

wave frequencies, an optimization process has to be carried out in irregular seas in a future work. Thereby, the system parameters have to be optimized in such a way that the harvested power gets high for different peak frequencies, which are present in real open seas. This can be done, for example, by simulating the behavior of the mechanical system in different irregular seas with different peak frequencies and checking at which system parameters the sum of all harvested powers becomes high. Such an optimization process has been performed in [19] for a drifting sensor platform. Since only a few system parameters have to be optimized in this study, the gradient can be calculated via finite difference methods. However, other gradient-based algorithms can also be used for the optimization of this nonlinear problem.

Moreover, required future work is the determination of an optimal damping strategy in order to adapt to the change of the dominant frequency of encounter waves.

Limitations of this work are the 2d analysis of the system and the missing hydrodynamic interaction forces between different CFBs. This can also be addressed in a future work by a 3D analysis using more sophisticated numerical tools, which however will lead to considerably higher computational costs.

5. Conclusions

In this work, a multibody wave energy converter consisting of a frame and several inclined modules is investigated. For this system, novel general equations of motion for an arbitrary number of involved CFBs are presented and the involved hydrodynamic forces are computed for regular and irregular waves. The harvested energy is studied for different numbers of CFBs and inclination angles. Since the harvested energy directly depends on the relative velocities between the CFBs and the frame, large and fast motions of the CFBs result in large amounts of harvested energy.

For the used system parameters, it has been found that a large amount of energy can be harvested in the presence of waves with corresponding high wave frequencies. However, in waves with low wave frequencies, a useful amount of energy can be harvested for a larger number of CFBs only. Thereby, a small inclination of the CFBs leads in general to more harvested energy than larger inclination angles. However, a varying angle leads to local maxima in the energy. This indicates that the inclination angle can have

an effect on the maximum amount of energy which can be harvested from regular and irregular waves.

Comparing the results for both cases of excitations, it is shown that a larger amount of power can be harvested from regular waves than from irregular waves. However, the harvested energy from irregular waves is less sensitive against changes in the system and wave parameters.

It can be summarized that large amounts of energy can be harvested from the multibody wave energy converter for higher wave frequencies. However, since in the real ocean waves with low frequencies occur, an optimization process has to be performed in order to increase the harvested energy in real seas. Thereby, inclination angles should be taken into account, as they can have an effect on the maximum amount of energy which can be harvested. In the optimization process, the inclination angle and the size of the CFBs have to be optimized together, as different inclination angles can lead to different optimal cylinder sizes. Here, irregular sea has to be considered, as it is the relevant realistic case and leads to different amount of harvested power as in regular sea.

Acknoledgements

We thank the anonymous reviewers for suggestions for future work.

References

[1] M. E. McCormick, Ocean wave energy conversion, Courier Corporation, 2013.

[2] V. Vaziri, A. Najdecka, M. Wiercigroch, Experimental control for initiating and maintaining rotation of parametric pendulum, The European Physical Journal Special Topics 223 (4) (2014) 795–812. doi:10.1140/epjst/e2014-02141-y.

[3] D. Yurchenko, P. Alevras, Parametric pendulum based wave energy converter, Mechanical Systems and Signal Processing 99 (2018) 504–515. doi:10.1016/j.ymssp.2017.06.026.

[4] L. Dostal, M.-A. Pick, Power generation of a pendulum energy converter excited by random loads, in: 9th European Nonlinear Oscillations Conference, ENOC 2017, 2017.

[5] L. Dostal, K. Korner, E. Kreuzer, D. Yurchenko, Pendulum energy converter excited by random loads (2018). doi:10.1002/zamm.201700007.

[6] R. Waters, M. Stålberg, O. Danielsson, O. Svensson, S. Gustafsson, E. Strömstedt, M. Eriksson, J. Sundberg, M. Leijon, Experimental results from sea trials of an offshore wave energy system, Applied Physics Letters 90 (3) (2007) 034105. doi:10.1063/1.2432168.

[7] H. Polinder, M. E. Damen, F. Gardner, Linear PM generator system for wave energy conversion in the AWS, IEEE transactions on energy conversion 19 (3) (2004) 583–589. doi:10.1109/TEC.2004.827717.

[8] B. Drew, A. R. Plummer, M. N. Sahinkaya, A review of wave energy converter technology, Proceedings of the Institution of Mechanical Engineers, Part A: Journal of Power and Energy 223 (8) (2009) 887–902. doi:10.1243/09576509JPE782.

[9] E. Lejerskog, C. Boström, L. Hai, R. Waters, M. Leijon, Experimental results on power absorption from a wave energy converter at the Lysekil wave energy research site, Renewable energy 77 (2015) 9–14. doi:10.1016/j.renene.2014.11.050.

[10] K. Budar, J. Falnes, A resonant point absorber of ocean-wave power, Nature 256 (5517) (1975) 478–479.

[11] D. Evans, A theory for wave-power absorption by oscillating bodies, Journal of Fluid Mechanics 77 (1) (1976) 1–25. doi:10.1017/S0022112076001109.

[12] C. C. Mei, Power extraction from water waves, Journal of Ship Research 20 (02) (1976) 63–66.

[13] C. Liang, L. Zuo, On the dynamics and design of a two-body wave energy converter, Renewable energy 101 (2017) 265–274. doi:10.1016/j.renene.2016.08.059.

[14] M. Hollm, L. Dostal, D. Yurchenko, R. Seifried, Performance increase of wave energy harvesting of a guided point absorber, The European Physical Journal Special Topics (2022). doi:10.1140/epjs/s11734-022-00497-7.

[15] S. J. Beatty, M. Hall, B. J. Buckham, P. Wild, B. Bocking, Experimental and numerical comparisons of self-reacting point absorber wave energy converters in regular waves, Ocean Engineering 104 (2015) 370–386. doi:10.1016/j.oceaneng.2015.05.027.

[16] E. S. Hadi, M. Iqbal, A. Wibawa, O. Kurdi, et al., Experimental studies of interaction forces that affect the position of vertical plates on oscillating heave plates with cylindrical bodies in regular waves, International Journal of Renewable Energy Development 9 (1) (2020) 77–84. doi:10.14710/ijred.9.1.77-84.

[17] SINN Power: OHP platform (13.05.2022).
URL `www.sinnpower.com/platform`

[18] P. Famouri, W. R. Cawthorne, N. Clark, S. Nandkumar, C. Atkinson, R. Atkinson, T. McDaniel, S. Petreanu, Design and testing of a novel linear alternator and engine system for remote electrical power generation, in: IEEE Power Engineering Society. 1999 Winter Meeting (Cat. No. 99CH36233), Vol. 1, IEEE, 1999, pp. 108–112. doi:10.1109/PESW.1999.747434.

[19] J. Harms, M. Hollm, L. Dostal, T. A. Kern, R. Seifried, Design and optimization of a wave energy converter for drifting sensor platforms in realistic ocean waves, Applied Energy 321 (2022) 119303. doi:10.1016/j.apenergy.2022.119303.

[20] J. N. Newman, Marine hydrodynamics, The MIT press, 2018.

[21] R. W. Yeung, Added mass and damping of a vertical cylinder in finite-depth waters, Applied Ocean Research 3 (3) (1981) 119–133. doi:10.1016/0141-1187(81)90101-2.

[22] C. Garrett, Wave forces on a circular dock, Journal of Fluid Mechanics 46 (1) (1971) 129–139. doi:10.1017/S0022112071000430.

[23] L. Dostal, E. Kreuzer, Probabilistic approach to large amplitude ship rolling in random seas, Proceedings of the Institution of Mechanical Engineers, Part C: Journal of Mechanical Engineering Science 225 (10) (2011) 2464–2476. doi:10.1177/0954406211414523.

[24] L. Dostal, E. Kreuzer, N. Sri Namachchivaya, Non-standard stochastic averaging of large-amplitude ship rolling in random seas, Proceedings of the Royal Society A: Mathematical, Physical and Engineering Sciences 468 (2148) (2012) 4146–4173. doi:10.1098/rspa.2012.0258.